metals

MDPI

Article

Friction Behavior and Self-Lubricating Mechanism of SLD-MAGIC Cold Worked Die Steel during Different Wear Conditions

Hongqing Wu [1,2], Hong Mao [1,2], Hui Ning [1,2], Zhipeng Deng [1,2] and Xiaochun Wu [1,2,*]

[1] School of Materials Science and Engineering, Shanghai University, Shanghai 200444, China; wuhongqing@shu.edu.cn (H.W.)
[2] State Key Laboratory of Advanced Special Steel, Shanghai University, Shanghai 200444, China
* Correspondence: xcwu@staff.shu.edu.cn

Abstract: Wear tends to shorten tool life, reduce component quality. To prevent or postpone the wear of tool steel forming tools, methods to increase wear resistance, such as increasing the material hardness, optimizing the carbide distribution and application of surface coatings, are often used. However, the formation of lubricating phases in steels leading to anti-attrition is less investigated. The friction behavior of three steels were investigated thoroughly by a tribo test with different normal loads. A Field-emission scanning electron microscope (FE-SEM) along with energy dispersive X-ray spectroscopy (EDS) were used to characterize the microstructure as well as the influence of the precipitated phases on the wear mechanisms. Results showed the friction coefficient decreased with increasing normal load, whereas the wear rate increased with increasing normal load. Compared with SKD11 and DC53 steels, the friction coefficient and wear volume of SLD-MAGIC steel were reduced by 0.1 to 0.3 and 10% to 30%, respectively. With the increase of normal load, the wear mechanism changed in order from abrasive wear, adhesive wear to oxidation wear. The more carbide contents, the rounder the carbide, the better the wear resistance of the tool steel. It can be shown that, under different normal loads, SLD-MAGIC exhibits better wear performance than SKD11 and DC53 tool steels, which is mainly due to the self-lubricating phenomenon of SLD-MAGIC steel. The self-lubricating mechanism was due to the fact that the exfoliated sulfide during wear formed a lubricating film to reduce wear.

Keywords: SLD-MAGIC cold worked die; sulfide phase; carbide phase; self-lubricating; wear mechanism

Citation: Wu, H.; Mao, H.; Ning, H.; Deng, Z.; Wu, X. Friction Behavior and Self-Lubricating Mechanism of SLD-MAGIC Cold Worked Die Steel during Different Wear Conditions. *Metals* **2023**, *13*, 809. https://doi.org/10.3390/met13040809

Academic Editors: Slobodan Mitrovic, Badis Haddag and Massimo Pellizzari

Received: 17 March 2023
Revised: 8 April 2023
Accepted: 18 April 2023
Published: 20 April 2023

1. Introduction

Cold worked die steels are widely used in the production of tool products, such as blanking and piercing die, trimming die, punch, scissors, cold extruding die, pressing and bending die, drawing die, punching and drawing die, etc. [1]. However, the die surface is often subjected to tensile stress or compressive stress, friction force and impact, which lead to the overload, fatigue and wear of the die surface and subsequently cause die premature failure. Wear, as the main failure mode in cold worked die (accounting for nearly 80% of failure cases [2,3]), is normally divided into abrasive wear, adhesive wear and oxidation wear [4]. As numerous studies reported [5,6], the different wear mechanisms are related to material properties and wear conditions. Material properties such as chemical composition, hardness and microstructure directly affect the wear behavior of steel. In addition, the wear conditions, such as normal loads and lubrication conditions, play a critical role with regards to the material wear performance. Thus, how to enhance the wear resistance of cold worked die steel is the key to improving the surface quality of the formed products and extending die service life.

Normally, the common approaches to minimizing wear and extending die service life are: (i) enhancing the wear resistance of cold worked die steel by micro-alloy, i.e.,

adding alloy elements which are beneficial for improving wear resistance, (ii) selecting a suitable heat treatment process to optimize the microstructure and improve mechanical properties, (iii) using surface modification techniques like nitriding treatment and thermal diffusion (TD) carbide treatment and physical vapor deposition (PVD) on the die surface to modify the wear resistance [7–9]. In Linhu Tang et al. [10], the influence of different hardness levels obtained by different heat treatment processes on the friction and wear performance and mechanism was investigated. It showed that the wear rate of D2 steel decreased with increasing hardness and tended to be highest at hardness values of 65 HRC. Sunil Kumar et al. [11] investigated the wear behavior of SKD-11 and SKD-61 tool steels with a similar hardness to 50 HRC, and found that the SKD-61 exhibited a better wear performance than that of the SKD-11 under high load and high sliding velocity conditions. B.F. Zappelino et al. [12] Studied the tribological behavior by investigation of the impact of a combination of deep cryogenic treatment, pulsed plasma nitriding and a multilayer film TiC-N/AlTiN/CrAlTiN/CrN on P/M cold worked tool steel Vanadis 10, and found that the Vanadis 10 presented higher dry sliding wear resistance in all tested conditions. In addition, a new cold worked tool steel named S-MAGICTM was developed by Kunichika Kubota [13]. Unlike the traditional idea of improving the wear resistance of cold worked die steel, it was proved that the addition of S and Cu in S-MAGICTM could form the self-lubricating phase to obtain the wear reduction ability during the HTSS (high tensile strength steel) process. However, the influence of the self-lubricating phase on the wear resistance of cold worked die steel was still not well understood. Thus, it is necessary to investigate friction behavior of SLD-MAGIC cold worked die steel during different wear conditions, and to get a deeper understanding of the influence of self-lubricating phase on the wear mechanism of SLD-MAGIC cold worked die steel.

The aim of the current work is to investigate the influence of the precipitated phase structure on the wear behavior and wear mechanism of cold worked die steel. Focus is placed on the study of the size and distribution of carbides and sulfides on wear behavior. Microstructures at different length scales were characterized by using FE-SEM along with EDS and JMatPro 7.0 software. The results of this study could be a further investigation on the self-lubricating mechanism of SLD-MAGIC steel, and a new guide for designing of alloying mechanism of anti-friction materials.

2. Materials and Methods

The present study was focused on three different commercial tool steels, i.e., SKD11, DC53 and SLD-MAGIC cold worked die steels (China, Dongguan, Hitachi Metal (Dongguan) Special Steel Co. LTD). These were delivered in the shape of forged plates in a soft annealed condition. The chemical composition of these tool steels is tabulated in Table 1.

Table 1. Chemical composition and hardness of tool steels used in the study.

Steel	Chemical Composition (wt%)												Hardness (HRC)
	C	Si	Mn	Cr	Mo	V	W	Ni	Cu	Al	P	S	
SKD11	1.46	0.34	0.24	11.6	0.97	0.30	\	\	\	\	0.02	0.003	62.7
DC53	1.05	0.96	0.33	8.12	2.18	0.35	\	\	\	\	0.02	0.002	61.5
SLD-MAGIC	1.07	0.93	0.46	8.09	0.93	\	0.28	0.43	0.40	0.25	0.02	0.097	61.3

The experimental material is sampled from the core of the ingot. Figure 1 shows the treatment conditions of the conventional process to quench and temper the samples from the tool steels. Hardness of the investigated samples was measured using a Rockwell-C machine (China, Shanghai, Shanghai Zhujin Analytical Instrument Co., Ltd., Willson-Rockwell, RB 2000). For each test specimen, at least five measurements were performed and average value calculated, and the final values are indicated in the last column of Table 1.

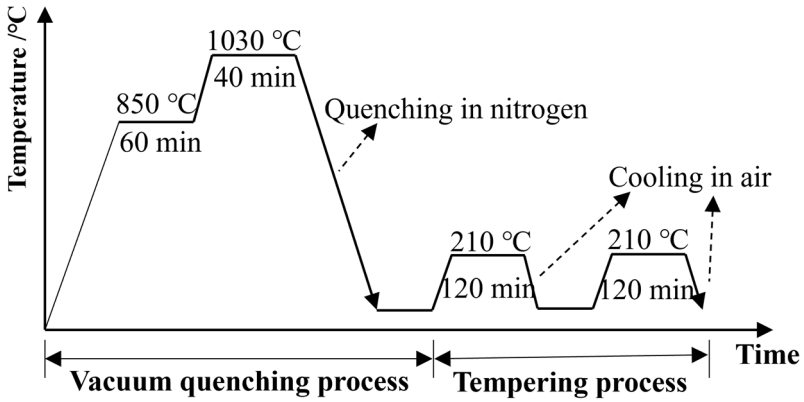

Figure 1. The conventional quenching/tempering process of cold worked die steels.

In order to evaluate the wear resistance, heat treated samples were subjected to round sliding wear tests under atmospheric dry sliding conditions with the ball-to-disk configuration. All tests were performed on a wear testing machine (China, Jina, Jinan Test Gold Group Co., Ltd., DX-NPO11 POD) at room temperature. The friction counterbody was a polished ball (China, Heze, Yuncheng Kangda Steel Ball Co., Ltd., G5) made of GCr15 steel with a diameter of 5 mm and a hardness of 64-66 HRC. In each friction experiment took place under a different normal load for each steel, and a new steel ball with an unworn surface was used. The sample size was a disc with a diameter of 20 mm and a thickness of 3 mm, and the roughness Ra of the sample polished by sandpaper was controlled at 0.7~0.8 μm. The tribological tests were performed by sliding with the radius of the friction track of 4 mm, the linear speed of 0.2 m/s, the sliding time of 1 h and different normal loads of 10 N, 40 N and 70 N. The coefficient of friction was measured continuously through a load cell measuring the tangential force. An optical profilometer (China, Hong Kong, Bruker Scientific Instruments Hong Kong Co., Ltd., Contour GT-K) was used to measure the two-dimensional depth and width of the wear marks and the three-dimensional morphology of the wear marks, and the wear volume was calculated.

Heat treated samples from three tool steels were cut, polished and etched with 10% Nital (10 mL HNO_3 + 90 mL ethanol). The microstructure of etched metallographic specimens was analyzed by a metallographic microscope (Japan, Tokyo, Nikon Corporation, MA100). A field-emission scanning electron microscope (FE-SEM, Germany, Oberkochen, Carl Zeiss AG, Supra-40 type) with energy dispersive X-ray spectroscopy (EDS) at 15 kV was also used to detailed identify the microstructural features and phases and investigate the wear surfaces and sections along the sliding direction. The elemental distribution of the wear surface was characterized using EDS. Size distribution and volume fraction of carbides were evaluated using SEM and Image-pro Plus 6.0 software (China, Shanghai, Media Cybernetics Shanghai representative office) at a magnification of 10,000×. JMatPro 7.0 software (China, Shanghai, CnTech Co., Ltd.) was used for phase stability calculation.

3. Results

3.1. Analysis of Structural Characteristics

Figure 2a–f shows the microstructure of the heat-treated tool steels. The tempered microstructure of the three steels consists of a martensitic matrix decorated with considerable carbides, including primary eutectic carbides (ECs) and secondary carbides (SCs) (Figure 2b,d,f). The types of the primary and secondary carbides are (Fe, Cr)xCy, as confirmed by EDS microanalysis in Table 2. The primary carbide particles precipitated during solidification in steel and the formation of secondary carbides occurred during tempering of the steel, which are smaller in size. The combination of these carbides enhances the hardness and wear resistance of tool steel [14].

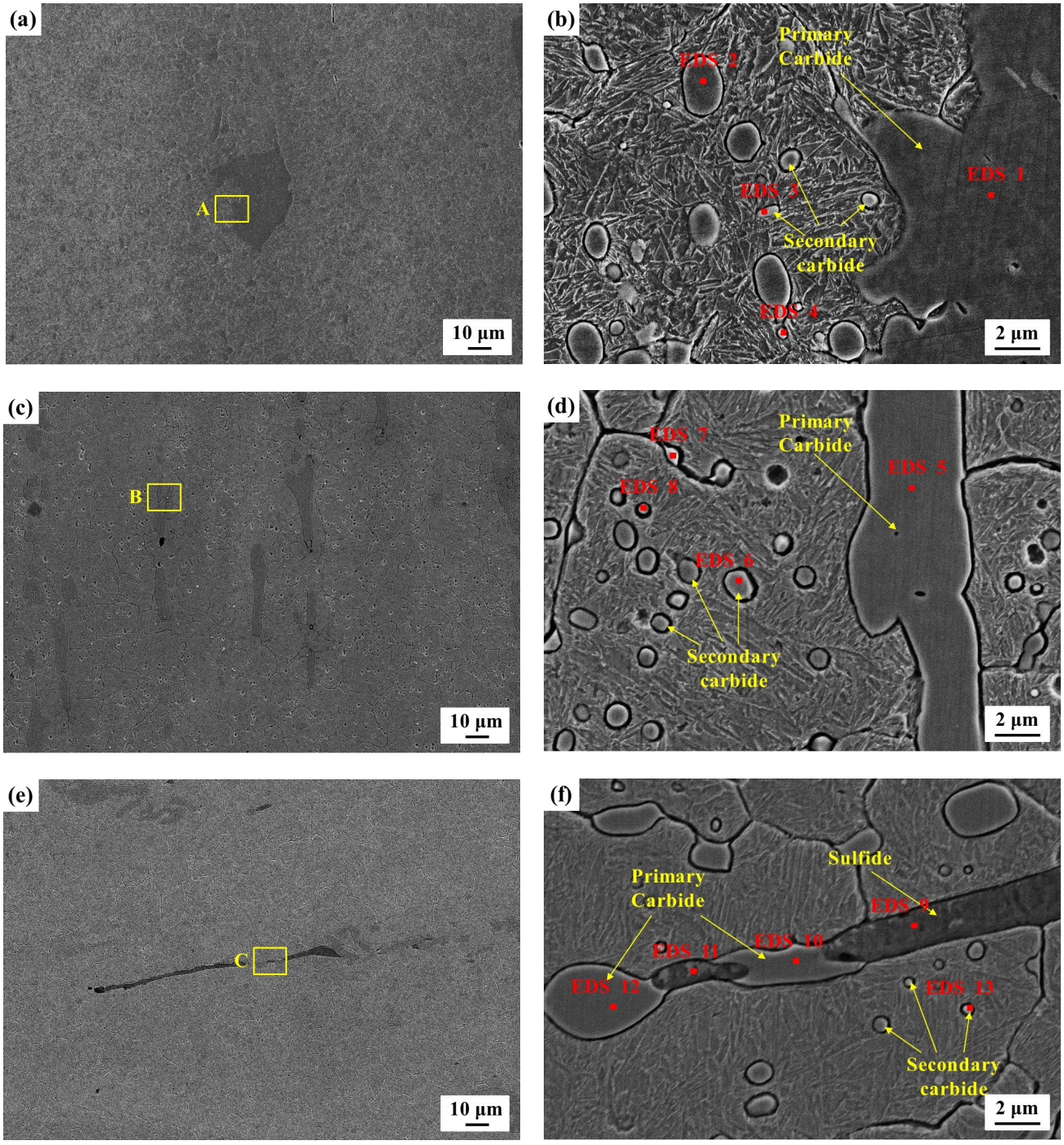

Figure 2. SEM micrographs of the tempered steel: (**a**) SKD11; (**b**) enlarged image at A in Figure 2a; (**c**) DC53; (**d**) enlarged image at B in Figure 2c; (**e**) SLD-MAGIC; (**f**) enlarged image at C in Figure 2e.

Differences are seen in the size and uniformity of the distribution of carbides. SKD11 steel contains large heterogeneously distributed primary carbides, Figure 2a. The width of the carbides ranged from 20 to 30 μm with a length in the range of approximately 50 μm. Compared with SKD11 steel, SLD-MAGIC steel and DC53 steel have a smaller size of the primary carbide, with lengths from 10 to 20 μm and widths from 5 to 10 μm. In addition, SLD-MAGIC has a certain amount of elongated sulfide of type (Fe, Mn, Mo)xSy (Table 2). Apart from that, we found that some of the carbides precipitated at the boundaries of the sulfides, in other words, they precipitated symbiotically.

Table 2. The atomic percentage of tool steels used in the study in SEM images by EDS.

Point	Fe	Cr	V	Mo	S	Mn
1	36.8	37.6	0	14.4	-	-
2	41.8	44.2	1.1	0.9	-	-
3	60.6	24.8	-	3.9	-	-
4	58.3	22.0	0.4	4.9	-	-
5	34.9	33.5	5.5	11.7	-	-
6	35.7	36.6	4.0	9.6	-	-
7	47.7	4.6	1.6	30.3	-	-
8	26.0	43.1	4.0	5.9	-	-
9	8.1	3.4	0.4	4.3	26.6	41.1
10	37.9	48.1	-	1.6	-	-
11	4.5	2.0	0.8	0.6	26.8	50.4
12	35.8	46.2	0.7	2.6	-	-
13	54.6	33.7	-	1.9	-	-

3.2. Statistics and Analysis of Carbides

Thermodynamic calculations using JMatPro 7.0 software were made to evaluate and predict the stability and type of carbides, as shown in Figure 3. The main types of carbides predicted to exist in the investigated steel are $M_{23}C_6$ and M_7C_3, and M_2C, MC and M_6C also exist during solidification. The equilibrium carbides at 1030 °C can be approximated as the primary carbides in the quenched microstructure, and the equilibrium carbides at 210 °C can be approximated as the carbides in the specimen after tempering at 210 °C. Then, subtracting the equilibrium carbide content in the steel at 1030 °C from the equilibrium carbide content at 210 °C gives the secondary carbide content in the structure after tempering at 210 °C. As shown in Table 3, the total carbide content of SKD11, DC53 and SLD-MAGIC steels as well as the contents of primary carbide, secondary carbide and various carbides under the condition of quenching at 1030 °C and tempering at 210 °C are shown. In addition, it can be seen from Figure 3c that there is a banded (Mn, Fe, Mo)xSy sulfide phase in SLD-MAGIC steel, and its mass fraction is 0.26%.

Table 3. Mass fraction of equilibrium phase calculated by JMatPro 7.0 software (wt%).

Steel	All Carbides	Primary Carbide	Secondary Carbide				
			M_7C_3	M_6C	$M_{23}C_6$	MC	Total
SKD11	16.8	10.0	2.8	0	3.3	0.7	6.8
DC53	15.2	5.2	0.1	0	9.5	0.4	10.0
SLD-MAGIC	15.1	5.8	3.9	0.2	5.23	0	9.3

Size distribution and volume fraction of the carbides, determined on twenty randomly scanned images under different fields of view, were evaluated using SEM and Image-pro Plus 6.0 software, performed at a magnification of 10,000× (Figure 4). The size distribution of the particles is presented with the equivalent circular diameter (ECD). In the case of a heat-treated specimen of SLD-MAGIC, on average ~1496 particles were found within the analyzed area (Figure 4a). On the other hand, for heat-treated specimens of SKD11and DC53, about 1647 and 2849 particles were found, respectively, within the same analyzing area size. As shown in Figure 4b, the total volume fractions of carbides were estimated as 12.79%, 11.2% and 10.5% for SKD11 steel, SLD-MAGIC steel and DC53 steel, respectively.

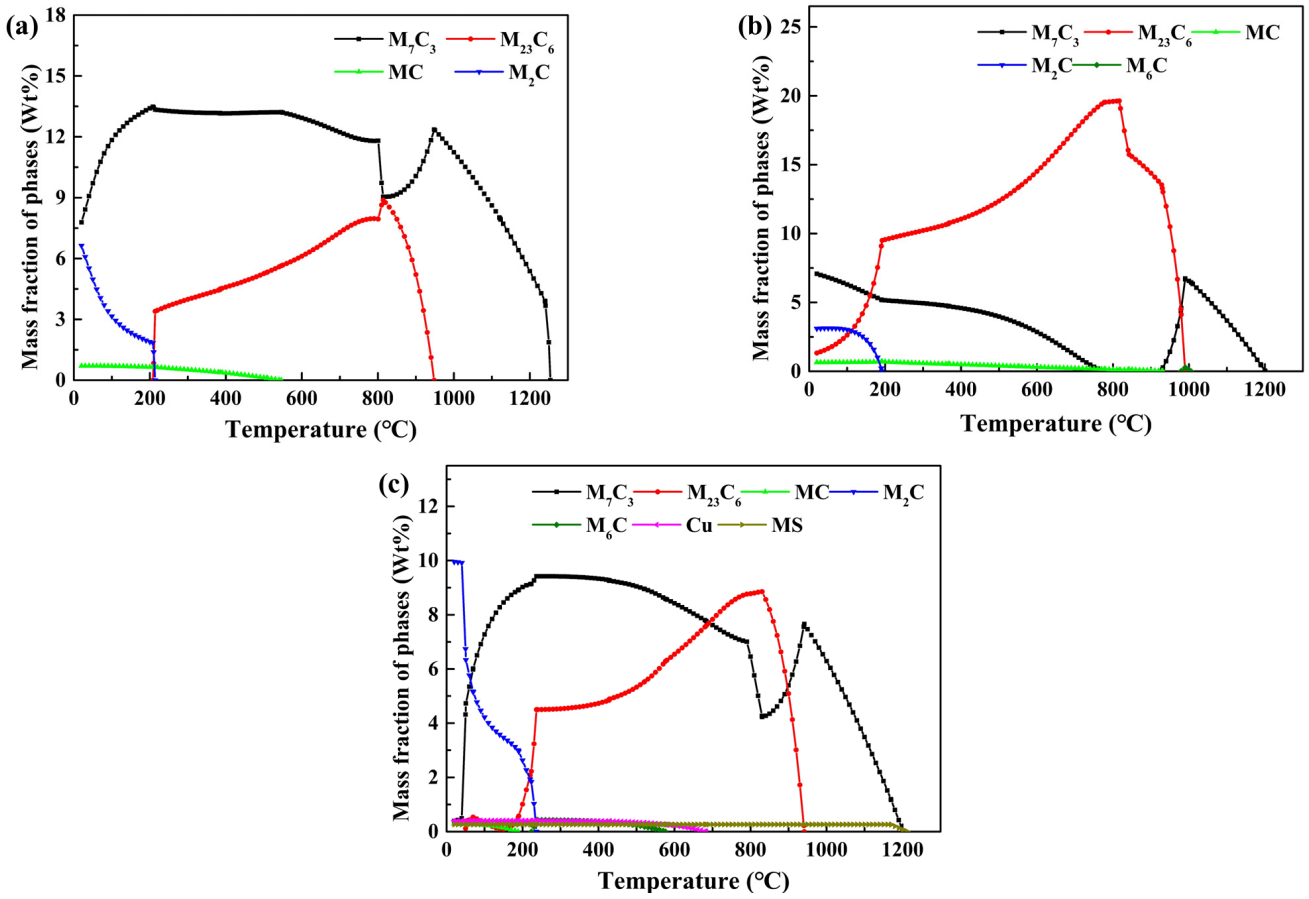

Figure 3. Calculation of equilibrium phase content with temperature: (**a**) SKD11; (**b**) DC53; (**c**) SLD-MAGIC.

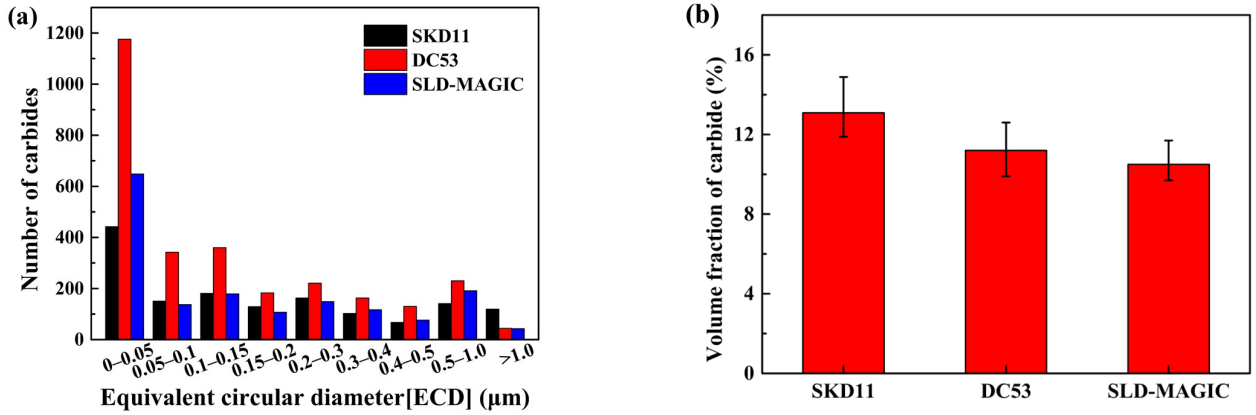

Figure 4. (**a**) Particle sizes distribution; (**b**) volume fraction of carbides of tempered SKD11, DC53 and SLD-MAGIC.

A large number of very fine particles (above 630) were detected in the specimen of SLD-MAGIC, while the largest number (above 1180) was detected in the DC53, and the smallest number (above 440) was detected in the SKD11, with the ECD size being lower that 0.05 μm. There is an almost constant number of particles with an ECD size from 0.05 to 0.15 μm (100–350), which then significantly decreased as the particles become larger, as shown in Figure 4a. In the same size range, DC53 has the largest number of particles, while SLD-MAGIC and SKD11 are almost the same.

3.3. Performance of Wear Resistance

3.3.1. The Friction Coefficient

Figure 5 shows the evolution of the friction coefficient (COF) versus the sliding time diagram for the tested tool steels for different normal loads of 10, 40 and 70 N. From the curves, it can be seen that the COF went through three stages: increasing, decreasing and stable. In the case of materials at all test conditions (Figure 5a–c) the COF during the running in first increases, which is followed by a slow decrease until it reaches the steady-state conditions. This can be attributed to the initial roughness of the surface that produces a momentary rise in friction, but when surface conformity and smoothing is achieved, the friction is reduced to a steady value. These average values of the stable stage were used to evaluate the galling for the tested tool steels, Figure 4b.

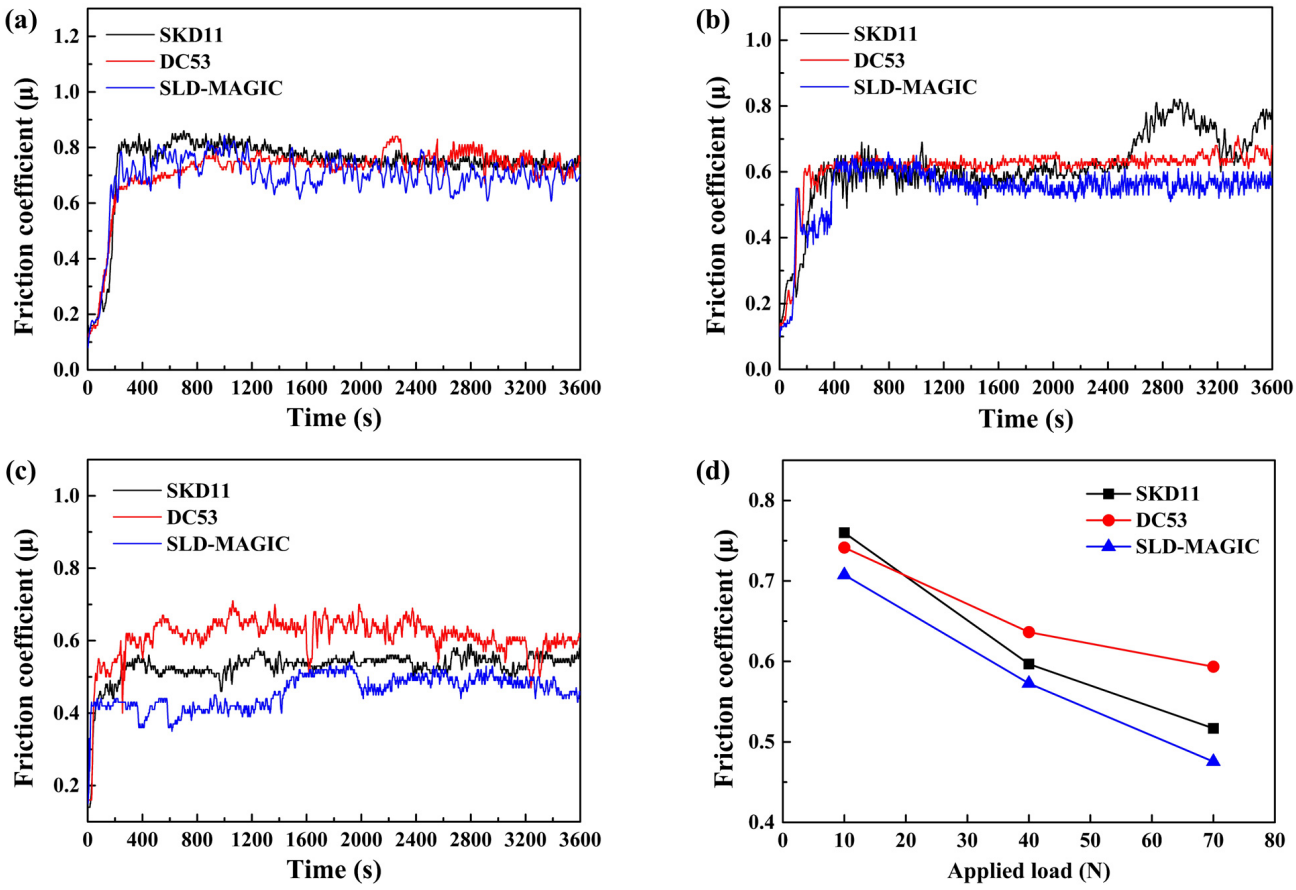

Figure 5. Variation in the friction coefficient with sliding time a normal load of (**a**) 10 N, (**b**) 40 N, (**c**) 70 N, and (**d**) average friction coefficients of three steels under different normal loads of 10 N, 40 N and 70 N.

When the sliding time was approximately 520 s, the friction coefficient of the three steels at 10 N increased to approximately 0.8, and then began to decrease slightly. At approximately 1200 s, the sliding friction process entered the relatively stable stage, and the friction coefficients of the three steels were approximately 0.75, 0.74 and 0.71. The friction coefficient of SLD-MAGIC fluctuates in a wide range, but SKD11 and DC53 tend to flatten. This may be due to the slightly lower hardness of SLD-MAGIC and the greater fluctuation of instantaneous friction coefficient due to the shedding of more hard particles under cyclic stress.

When the normal load is 40 N, the three steels reach the stage of stable friction at about 400 s. The friction coefficient of SKD11 is about 0.62, that of DC53 is about 0.59 and that of SLD-MAGIC is about 0.56. The significant fluctuation of the friction coefficient of

SKD11 is speculated to be caused by the metal adhesion of large particle carbide on the local contact surface during sliding friction, which is destroyed and then spalled in the subsequent relative sliding. When the normal load increases from 40 N to 70 N, the hard particles have shear with the substrate and the counter-abrasive body at the same time, that is, three-body friction and wear are formed. The fluctuation of the three-body friction and wear in the stable stage is smaller than that of two-body friction and wear [15].

As can be seen from Figure 5d, with the increase of the normal load, the average friction coefficient becomes smaller and smaller. This is because, with the increase of normal load, the wear surface and the micro-convexity of the grinding body are gradually worn out, which increases the wear area. Due to adhesive wear, the friction coefficient decreases to varying degrees, and the wear process is more stable. The friction heat accumulates gradually, which thickens the oxide film on the wear surface and reduces the adhesive force, thus reducing the friction coefficient.

3.3.2. The Wear Morphology

As can be seen from Figure 6, when the normal load is 10 N, the wear surfaces of the three steels have furrow-like wear marks parallel to the wear direction, showing obvious plastic deformation, so the wear mechanism is mainly abrasive wear caused by the behavior of "micro-ploughing" on the micro-convex body on the friction pair. In the sliding process, the carbide particles shear the matrix. As the hardness of the carbide particles is higher than that of the matrix, several furrows are left on the worn surface. Compared with SKD11 and DC53 steel, SLD-MAGIC has the least number of surface "furrows", the shallowest depth of wear scars, while SKD11 has a denser distribution of furrows. From Figure 6b, it is found that there are local oxidations on the wear surface of SKD11, which are mainly due to the large number of primary carbides in SKD11 bearing a higher compressive stress than the matrix during the grinding process, resulting in more instantaneous friction heat. The EDS data in Table 4 show the atomic percentage of carbide and oxide in Figure 6b. With the increase of the sliding time, the affinity of the Cr element enriched in the carbides and the O element was higher than that of the Fe element, so that the carbides will be oxidized before the substrate, and the oxidation degree of carbides is higher than that of the matrix.

Table 4. The atomic percentage of SKD11 in SEM images by EDS.

Point	Fe	O	Cr	V	Mo	S	Si
1	45.4	40.4	7.3	0	0	0	6.9
2	36.0	0	41.9	2.7	1.6	0	0.2

It can be observed from Figure 7 that, with the increase of normal load, the wear marks and furrows gradually widen, mainly because the number of micro-convex bodies on the friction surface and the real contact area increases, leading to the slow accumulation of friction heat and the softening and melting of the surface metal. With the further increase of friction time, grinding gradually falls off under the action of stress. In summary, when the normal load is 40 N, the wear mechanism is mainly adhesive wear and slight oxidation wear.

When the normal load increases from 10 N to 40 N, it can be seen that the three steels underwent different degrees of adhesive wear. Compared to SLD-MAGIC, DC53 showed the most severe adhesive wear during sliding friction and a certain amount of spalling. Cracks perpendicular to the sliding direction were also found on the friction surfaces of DC53 and SLD-MAGIC steels. This is due to the high hardness of the abrasive chips, which plays the role of abrasive particles during the wear process and forms worm-shaped cracks on the wear surface, characteristic of micro-motion wear, which is the characteristic of fretting wear.

Figure 8 shows the 3D profiles and SEM images of the wear morphology of SKD11, DC53 and SLD-MAGIC worn for 1 h at 70 N. When the normal load is 70 N, the SEM

photos show that the wear marks and furrows further widen, indicating serious adhesive wear and oxidative wear. It can be observed that large areas of oxides are distributed in strips along the direction of friction to form an oxide film with cracks. The peeling of the oxide films of DC53 is more serious, while the peeling of the oxide films of SKD11 and SLD-MAGIC is relatively slight.

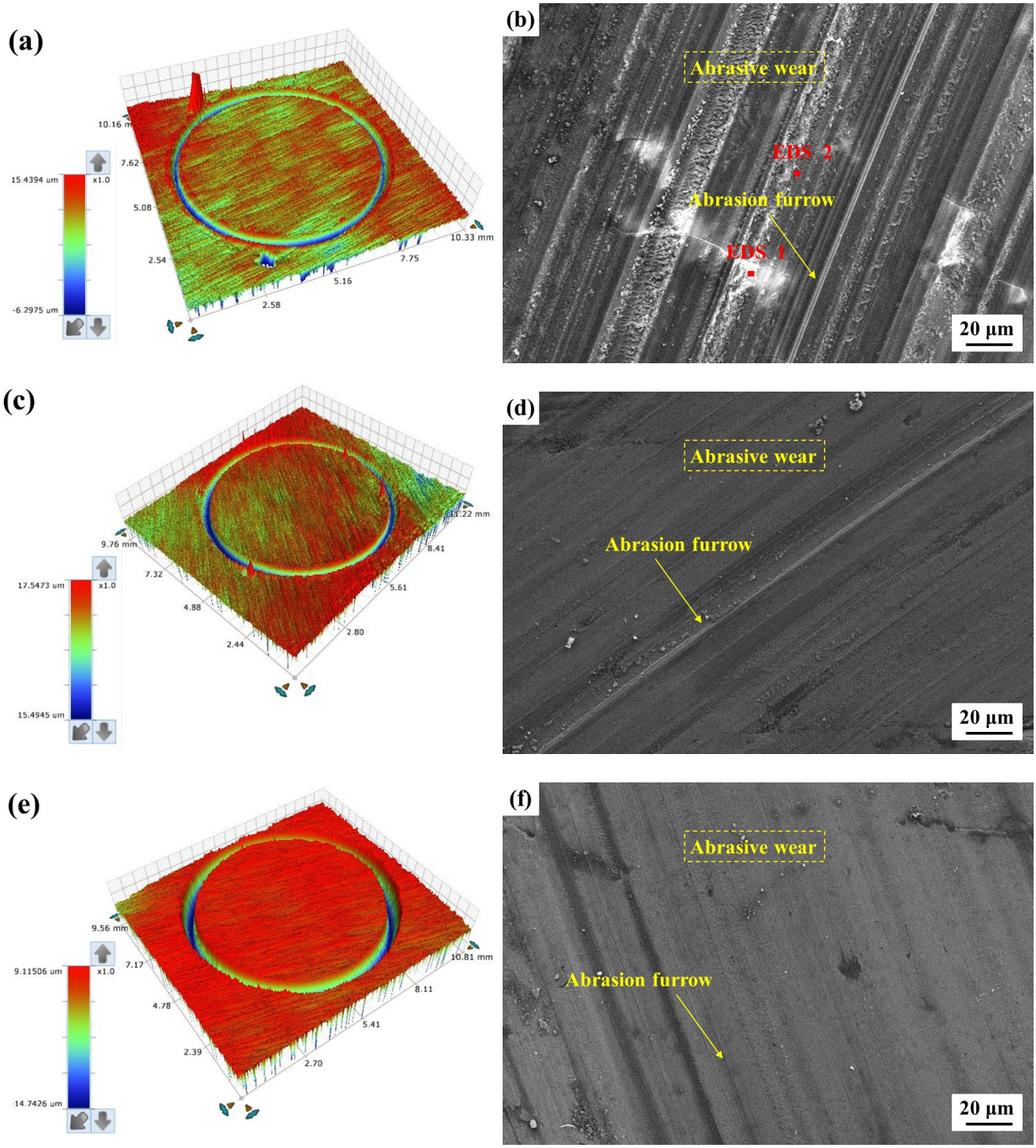

Figure 6. The 3D profile and the SEM images of wear morphology on the wear surface under a normal load of 10 N: (**a**,**b**) SKD11; (**c**,**d**) DC53; (**e**,**f**) SLD-MAGIC.

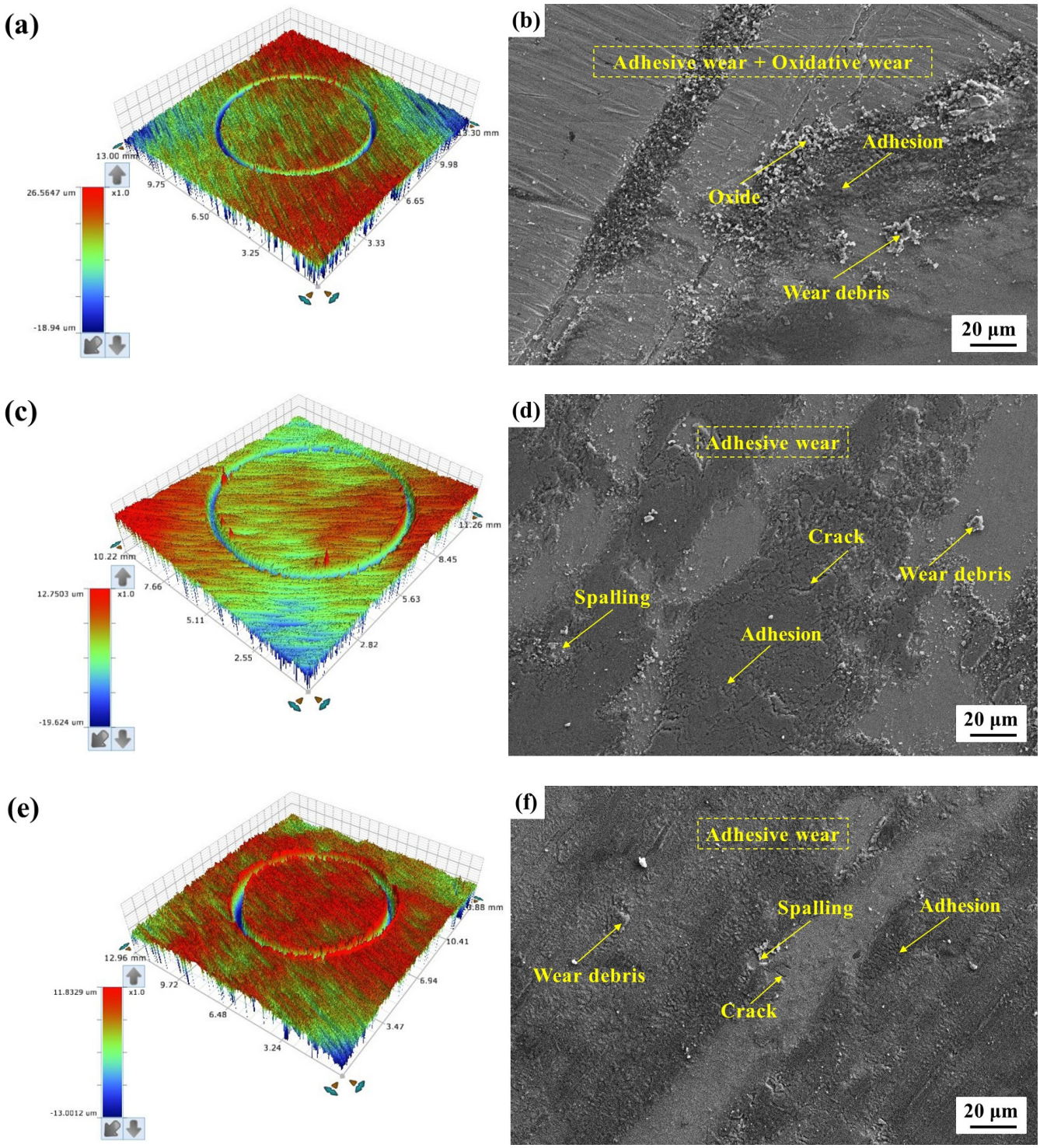

Figure 7. The 3D profile and the SEM images of wear morphology on the wear surface under a normal load of 40 N: (**a**,**b**) SKD11; (**c**,**d**) DC53; (**e**,**f**) SLD-MAGIC.

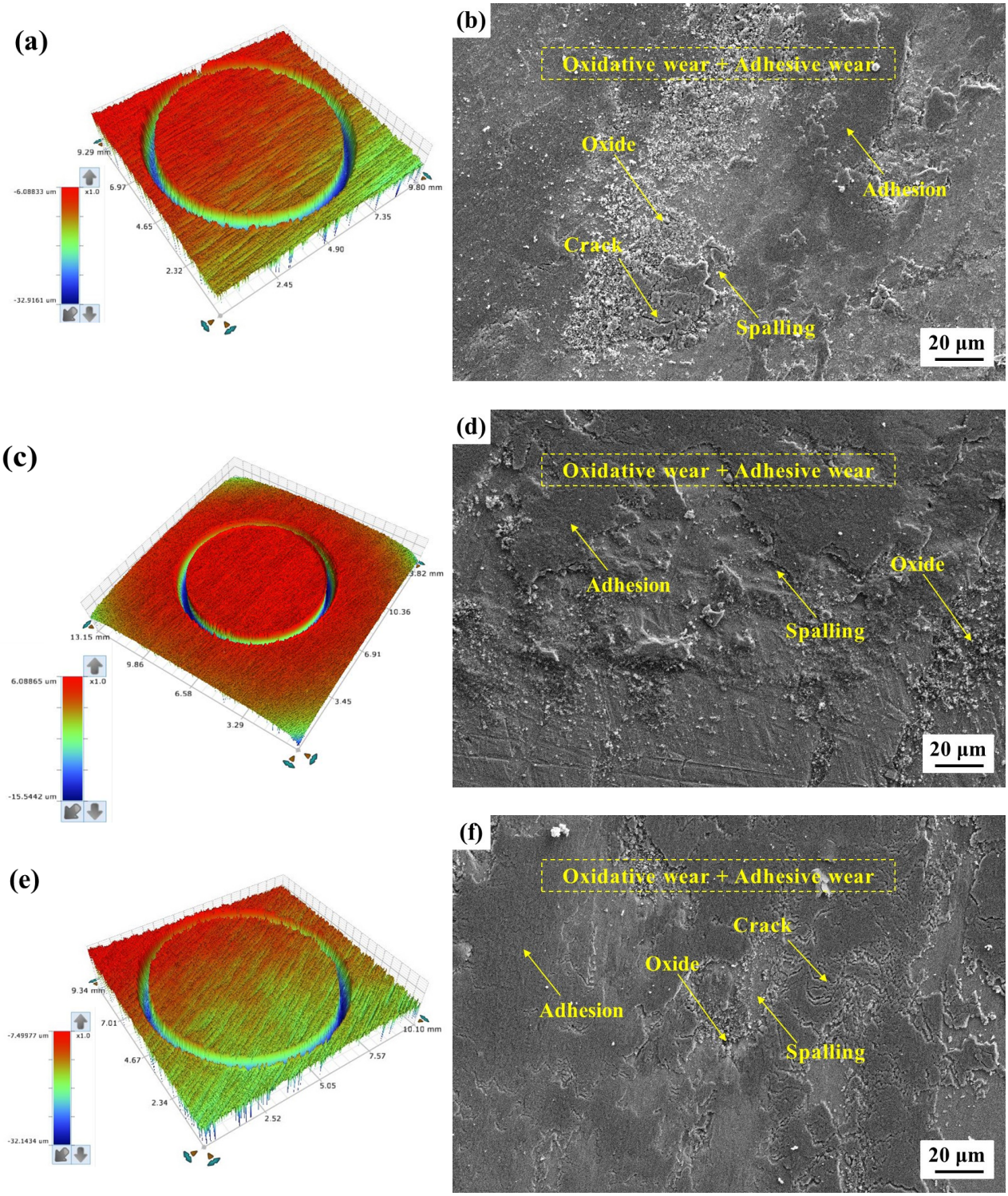

Figure 8. The 3D profile and the SEM images of wear morphology on the wear surface under a normal load of 70 N: (**a**,**b**) SKD11; (**c**,**d**) DC53; (**e**,**f**) SLD-MAGIC.

3.3.3. The Wear Volume

Figure 9 shows the wear volume of SKD11, DC53 and SLD-MAGIC under different normal loads of 10 N, 40 N and 70 N for 1 h. The wear volume increases with the increase of normal load, and there is no obvious linear relationship between wear volume and friction coefficient. When the normal load increases from 10 N to 40 N, the wear volume of the three steels is similar, and the wear volume of SLD-MAGIC is slightly better than that of

the other two steels; when the normal load is 40 N, the wear volume of SLD-MAGIC is 31.8% and 14.3% lower than those of DC53 steel and SKD11 steel, respectively; When the normal load is 70 N, the wear volume of SLD-MAGIC is 29.7% and 12.9% lower than those of DC53 steel and SKD11 steel, respectively. In general, SLD-MAGIC has the smallest wear volume and the best comprehensive wear resistance, followed by SKD11 and DC53.

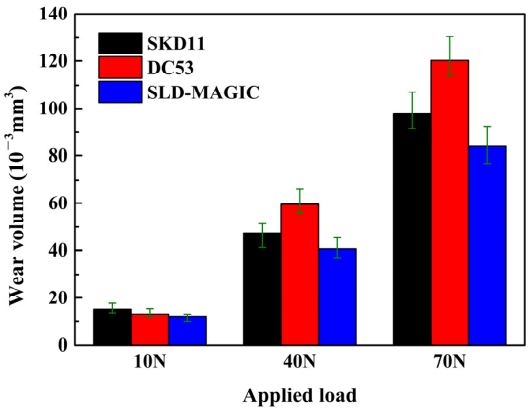

Figure 9. Wear volume of SKD11, DC53 and SLD-MAGIC steels under different normal loads of 10 N, 40 N and 70 N.

4. Discussion

4.1. Effect of Carbides on Wear Resistance

It has been reported that carbides have a great impact on the wear resistance of cold worked tool steels, which cannot just be explained completely by the total amount of carbides and is closely related to the type, amount, size and distribution of the carbides [16].

When the normal load is 10 N, the furrow generated by friction and wear is closely related to the size and shape of the carbide. The furrows caused by large particles of carbide are wider and deeper, while the relatively short free path of fine carbide leads to narrower and shallower furrows [17]. Large eutectic carbide has higher hardness, which can improve the wear resistance of steel, but irregular carbide particles can also aggravate abrasive wear. Figure 10 shows the abrasive wear mechanism. Figure 3 shows the number of carbides and the volume fractions of the primary and secondary carbides for the tested tool steels. The volume fraction of the primary carbides of SKD11 is 10%, which is 4.8% and 4.2% higher than those of DC53 and SLD-MAGIC, respectively. Because SKD11 has the largest amount and size of primary carbides, the furrow of SKD11 is wider and deeper. The wear resistance of SKD11 is slightly better than the other two steels at 10 N.

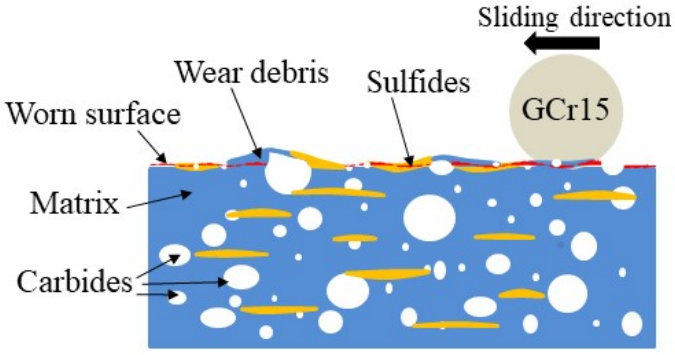

Figure 10. Schematic representation of the precipitation particle (carbides and sulfides) behavior during the pin-on-disc sliding wear test.

When the normal load is 40 N, the large particle size carbide can reduce the contact area between the two friction pairs during adhesive wear, thus reducing the adhesive spalling, while the smaller particle size carbide increases the contact area between the

matrix and the abrasive material, resulting in more severe adhesive wear, as shown in Figure 10. As can be seen from the statistical data in Figure 4, tempered SKD11 steel has 7% carbide >1 μm, which is higher than DC53 and SLD-MAGIC. It is reported that a larger number of secondary carbides can improve the galling resistance of cold work tool steels. Although the volume fractions of the primary carbides in DC53 and SLD-MAGIC were smaller compared with those in standard SKD11, the volume fractions of the secondary carbides were found to be larger by approximately 3.2% and 2.5%, respectively. As the content of secondary carbide precipitation is small when tempered at 200 °C, it can be seen from Figure 2 that the secondary carbide of SKD11 is only slightly less than that of the other two kinds of steel, Furthermore, the hardness of SKD11 after heat treatment is 1 HRC higher than that of DC53. Therefore, the wear resistance of DC53 is lower than that of SKD11 and SLD-MAGIC under the above circumstances.

4.2. Effect of Sulfides on Wear Resistance

According to the calculation of the phase diagram JMatPro 7.0 software, there are sulfides with a volume fraction of 4.5% in SLD-MAGIC steel. Through the wear scar morphology (Figure 11) and the energy spectrum (Table 5) under a normal load of 10 N, strip-shaped sulfide exfoliated pits on the surface of the sample were found. Figure 12 shows the morphology of the wear scar surface of the SLD-MAGIC steel at under a normal load of 40 N. There are sulfide-enriched areas on the worn surface discovered by EDS spectroscopy. It is well known that the shear strength of the sulfide is lower than that of the matrix [18]. The sulfides were shed under the action of cyclic stress with the increase of friction time. Because sulfide has low hardness and soft texture, the sulfide adhesive strips formed by exfoliated sulfide disperse on the wear surface during repeated friction, which not only effectively prevents the shearing action of carbide on the matrix, but also forms a film that can effectively reduce the adhesion between the contact points [19]. To sum up, the adhesive strips of sulfides play the role of lubrication and anti-friction, thus ensuring that SLD-MAGIC exhibits good anti-friction and wear properties.

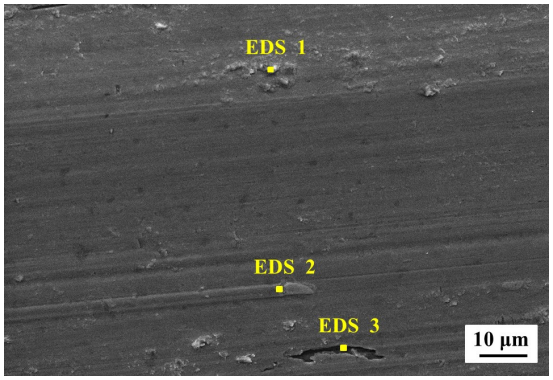

Figure 11. Wear morphology of SLD-MAGIC under a normal load of 10 N.

Table 5. The atomic percentage of SLD-MAGIC in SEM images by EDS.

Point	Mn	S	Fe	O	Cr	Mo
1	0	0	53.6	29.7	5.2	1.4
2	14.3	7.7	37.0	12.8	8.4	4.4
3	32.8	18.5	27.7	0	3.9	4.2

In order to further confirm the existence of the self-lubricating phenomenon of SLD-MAGIC steel in the process of friction and wear, a section of the worn sample under a normal load of 70 N is analyzed, as shown in Figure 13. Among them, the yellow line in Figure 13 is the position of the sample scanned in a straight line by SEM. Through the cross

section of the wear mark, there are sulfide exfoliation marks in the local area of the wear mark. Due to the low shear strength of the sulfide, the sulfide is very easy to peel off under a high normal load. The sulfide blocks the adhesion of the two contact points to a certain extent during the adhesive wear process, and forms a lubricating film in local areas, which reduces the material flaking in the process of adhesive wear. Combined with the friction and wear morphology of SLD-MAGIC, the adhesions exfoliated from the surface have not been further crushed, which is due to the lubrication of the exfoliated sulfides. Under different normal loads, SLD-MAGIC steel shows excellent friction and wear properties due to the existence of sulfides. The SLD-MAGIC steel exhibited excellent frictional wear properties due to the presence of sulfide under different normal loads.

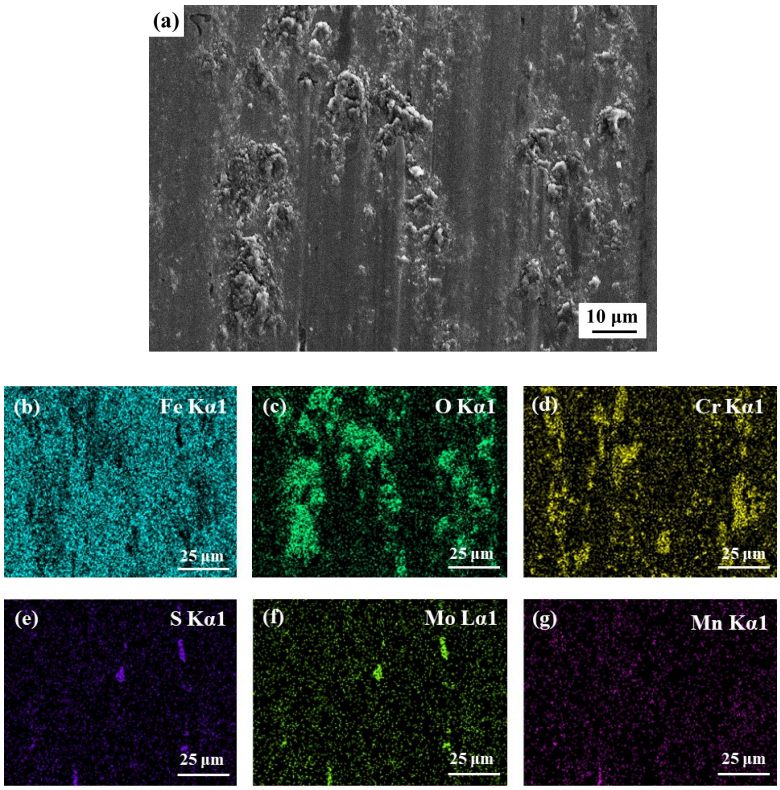

Figure 12. Wear morphology (**a**) and EDS elemental maps (**b**–**g**) of SLD-MAGIC under a normal load of 40 N.

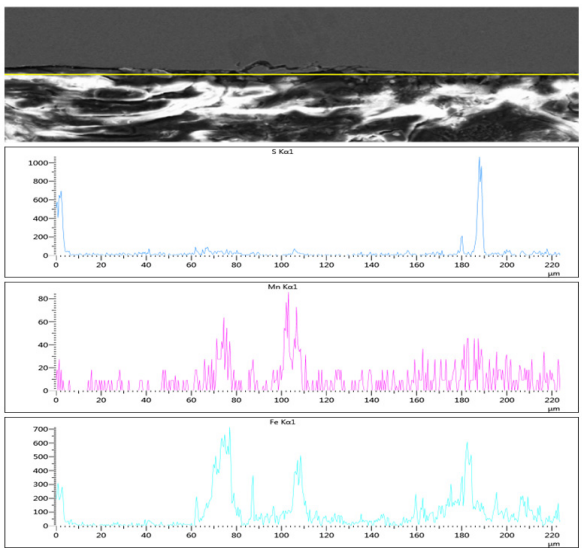

Figure 13. EDS analysis of the cross section of SLD-MAGIC for frictional wear under a normal load of 70 N.

4.3. Effect of Oxides on Wear Resistance

It was reported that the oxidation behavior of the steel surface considerably influenced the friction and wear behavior as well as the wear mechanism of the steel. First, the oxide film prevented direct contact between the counter-body and matrix, thus reducing the adhesion between them. Second, the oxide film formed in the friction and wear process of steel plays a lubricating role [20,21].

The morphology of the abrasion marks at 70 N showed the presence of a large number of white lumps, which are determined to be composed of Fe-rich oxides using EDS, as shown in Figure 14. With the increase of normal load and sliding time, the thickness of the oxide film increases, the strength of the oxide film tends to decrease and the oxide film flakes off in a scaly manner under the action of friction. Furthermore, a new oxide film is formed on the new worn surface. The repeated oxidation wear process will be carried out cyclically, resulting in an increase in the volume of oxidation wear. On the one hand, because the oxide has the characteristics of low strength and easy deformation, the oxide film plays the role of isolation and wear reduction; on the other hand, the oxide film can weaken the adhesion between metals in contact to a certain extent, reduce the adhesion wear and the friction coefficient.

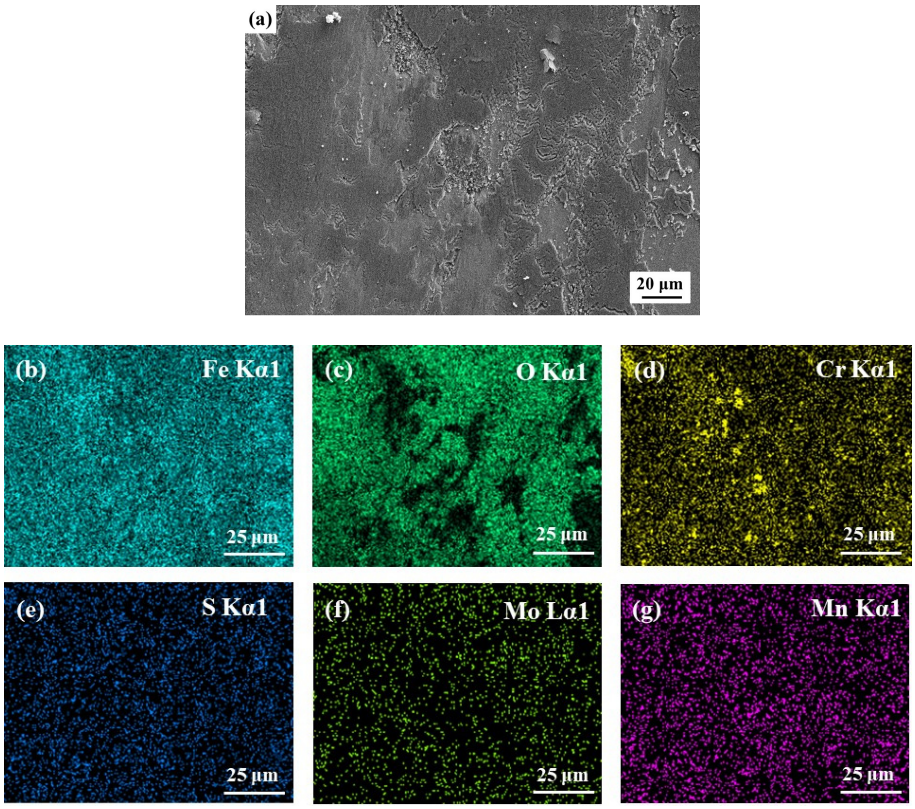

Figure 14. Wear morphology (**a**) and EDS elemental maps (**b**–**g**) of SLD-MAGIC under a normal load of 70 N.

5. Conclusions

In this paper, the combined effects of normal load, hardness, microstructure and precipitation on the friction coefficient, the wear volume and the wear mechanisms of three commercially available hardened tool steels with similar hardness were studied by dry friction and wear experiments. More importantly, the friction behavior and self-lubricating mechanism of SLD-MAGIC steel during circular reciprocating sliding wear against a GCr15 steel ball under different normal loads at room temperature were investigated by considering the effect of sulfide. Based on the results acquired, the following conclusions are drawn:

1. The tempered structure of SLD-MAGIC is composed of martensite matrix, coarse primary carbides, fine carbides and slender sulfides. Further, primary carbide and secondary carbide particles formed during heat treatment of the steel enhance the hardness and wear resistance of tool steel.
2. During circular reciprocating sliding of the tool steel and GCr15 steel ball, with the increase of normal load, the wear mechanism changed from abrasive wear to adhesive wear and then to oxidation wear.
3. The wear resistance of cold worked tool steel is closely related to the type, content, size and distribution of carbides. The total volume fraction of the primary carbides of SKD11 is 10%, which is 4.8% and 4.2% higher than those of DC53 and SLD-MAGIC, respectively, meanwhile, the volume fractions of the secondary carbides were found to be larger by approximately 3.2% and 2.5%, respectively. In addition, tempered SKD11 steel has 7% carbide >1 μm, which is higher than DC53 and SLD-MAGIC. Therefore, the higher the carbide content, the smaller the equivalent circular diameter (ECD) of the carbide, the better the wear resistance of the tool steel.
4. The SLD-MAGIC steel could realize self-lubrication and, compared with SKD11 and DC53 steel, the friction coefficient and wear volume of SLD-MAGIC steel were reduced by 0.1 to 0.3 and 10% to 30%, respectively, under the same normal load. The self-lubricating mechanism was that the sulfide with a volume fraction of 4.5%, which was easy to peel off under high normal load, forms a lubricating film in the local area, which played the role of lubrication and wear reduction, thus reducing the material spalling and reducing the wear volume.

Author Contributions: Conceptualization, X.W.; methodology, H.W.; software, H.W.; validation, H.M., H.N. and Z.D.; formal analysis, H.W.; investigation, H.N.; resources, H.M.; data curation, H.W.; writing—original draft preparation, H.W.; writing—review and editing, X.W.; visualization, Z.D.; supervision, H.W.; project administration, X.W.; funding acquisition, X.W. All authors have read and agreed to the published version of the manuscript.

Funding: This work is supported by National Key R&D Program of China (Grant Nos. 2016YFB0300400 and 2016YFB0300403).

Institutional Review Board Statement: Not applicable.

Informed Consent Statement: Not applicable.

Data Availability Statement: No data are reported.

Conflicts of Interest: The authors declare no conflict of interest.

References

1. Kara, F.; Küçük, Y.; Özbek, O.; Özbek, N.A.; Gök, M.S.; Altaş, E.; Uygur, İ. Effect of cryogenic treatment on wear behavior of Sleipner cold work tool steel. *Tribol. Int.* **2023**, *180*, 108301. [CrossRef]
2. Mashreghi, A.R.; Soleimani, S.M.Y.; Saberifar, S. The investigation of wear and corrosion behavior of plasma nitrided DIN 1.2210 cold work tool steel. *Mater. Des.* **2013**, *46*, 532–538. [CrossRef]
3. He, S.; Li, C.; Ren, J.; Han, Y. Investigation on Alloying Element Distribution in Cr_8Mo_2SiV Cold-Work Die Steel Ingot during Homogenization. *Steel Res. Int.* **2018**, *89*, 1800148. [CrossRef]
4. Cora, Ö.N.; Namiki, K.; Koç, M. Wear performance assessment of alternative stamping die materials utilizing a novel test system. *Wear* **2009**, *267*, 1123–1129. [CrossRef]
5. Soleimani, S.M.Y.; Mashreghi, A.R.; Ghasemi, S.S.; Moshrefifar, M. The effect of plasma nitriding on the fatigue behavior of DIN 1.2210 cold work tool steel. *Mater. Des.* **2012**, *35*, 87–92. [CrossRef]
6. Sulaiman, M.H.; Farahana, R.N.; Bienk, K.; Nielsen, C.V.; Bay, N. Effects of DLC/TiAlN-coated die on friction and wear in sheet-metal forming under dry and oil-lubricated conditions: Experimental and numerical studies. *Wear* **2019**, *438–439*, 203040. [CrossRef]
7. Trevisiol, C.; Jourani, A.; Bouvier, S. Effect of hardness, microstructure, normal load and abrasive size on friction and on wear behaviour of 35NCD16 steel. *Wear* **2017**, *388–389*, 101–111. [CrossRef]
8. Bourithis, L.; Papadimitriou, G.D.; Sideris, J. Comparison of wear properties of tool steels AISI D2 and O1 with the same hardness. *Tribol. Int.* **2006**, *39*, 479–489. [CrossRef]

9. Essam, M.A.; Shash, A.Y.; El-Fawakhry, M.K.; El-Kashif, E.; Megahed, H. Influence of micro-alloying elements and deep cryogenic treatment on microstructure and mechanical properties of S5 cold work shock resisting tool steel. *Results Mater.* **2023**, *17*, 100374. [CrossRef]
10. Tang, L.; Gao, C.; Huang, J.; Zhang, H.; Chang, W. Dry sliding friction and wear behaviour of hardened AISI D2 tool steel with different hardness levels. *Tribol. Int.* **2013**, *66*, 165–173. [CrossRef]
11. Kumar, S.; Ranjan Maity, S.; Patnaik, L. A comparative study on wear behaviors of hot work and cold work tool steel with same hardness under dry sliding tribological test. *Mater. Today Proc.* **2021**, *44*, 949–954. [CrossRef]
12. Zappelino, B.F.; de Almeida, E.A.d.S.; Krelling, A.P.; da Costa, C.E.; Fontana, L.C.; Milan, J.C.G. Tribological behavior of duplex-coating on Vanadis 10 cold work tool steel. *Wear* **2020**, *442–443*, 203133. [CrossRef]
13. Kubota, K.; Ohba, T.; Morito, S. Frictional properties of new developed cold work tool steel for high tensile strength steel forming die. *Wear* **2011**, *271*, 2884–2889. [CrossRef]
14. Das, D.; Dutta, A.K.; Toppo, V.; Ray, K.K. Effect of Deep Cryogenic Treatment on the Carbide Precipitation and Tribological Behavior of D2 Steel. *Mater. Manuf. Process.* **2007**, *22*, 474–480. [CrossRef]
15. Gultekin, D.; Uysal, M.; Aslan, S.; Alaf, M.; Guler, M.O.; Akbulut, H. The effects of applied load on the coefficient of friction in Cu-MMC brake pad/Al-SiCp MMC brake disc system. *Wear* **2010**, *270*, 73–82. [CrossRef]
16. Ko, D.-C.; Kim, S.-G.; Kim, B.-M. Influence of microstructure on galling resistance of cold-work tool steels with different chemical compositions when sliding against ultra-high-strength steel sheets under dry condition. *Wear* **2015**, *338–339*, 362–371. [CrossRef]
17. Bressan, J.D.; Daros, D.P.; Sokolowski, A.; Mesquita, R.A.; Barbosa, C.A. Influence of hardness on the wear resistance of 17-4 PH stainless steel evaluated by the pin-on-disc testing. *J. Mater. Process. Technol.* **2008**, *205*, 353–359. [CrossRef]
18. Li, C.; Deng, X.; Wang, Z. Friction behaviour and self-lubricating mechanism of low alloy martensitic steel during reciprocating sliding. *Wear* **2021**, *482–483*, 203972. [CrossRef]
19. Wu, J.; Wang, H.; Zhang, Z.; Wang, C.; Hou, Z.; Wan, S.; Wu, D.; Ouyang, X. High-pressure synthesis and performance analysis of WC-cBN-MoS_2 self-lubricating ceramic composites. *Int. J. Refract. Met. Hard Mater.* **2023**, *110*, 105989. [CrossRef]
20. Tong, Y.; Zhang, T.; Zhang, S. Influence of oxides on the formation of self-lubricating layer and anti-wear performance during sliding. *Tribol. Int.* **2023**, *179*, 108188. [CrossRef]
21. Yin, C.-H.; Yang, C.; Wu, Y.-Z.; Liang, Y.-L.; Zhu, Z.-L. Synergistic effect of cementite amorphization and oxidation on forming a nanocomposite self-lubricating surface during sliding. *Compos. Part B Eng.* **2022**, *236*, 109799. [CrossRef]